J. Electrochem. Sci. Eng. **00(0)** (2022) 000-000; http://dx.doi.org/10.5599/jese.1257

Open Access : : ISSN 1847-9286

www.jESE-online.org

Original scientific paper

Cerium-tricalcium phosphate coating for 316L stainless steel in simulated human fluid: Experimental, biological, theoretical, and electrochemical investigations

Hiba A. Abdulaah[1], Ahmed M. Al-Ghaban[1], Rana A. Anaee[1], Anees A. Khadom[2,✉] and Mustafa M. Kadhim[3,4,5]

[1]*Department of Materials Engineering, University of Technology, Baghdad, Iraq*
[2]*Department of Chemical Engineering, College of Engineering – University of Diyala – Baquba City 32001, Diyala governorate, Iraq*
[3]*Department of Dentistry, Kut University College, Kut, Wasit, 52001, Iraq*
[4]*College of Technical Engineering, The Islamic University, Najaf, Iraq*
[5]*Department of Pharmacy, Osol Aldeen University College, Baghdad, Iraq*

Corresponding author: ✉aneesdr@gmail.com

Received: January 27, 2022; Accepted: March 16, 2022; Published: April 27, 2022

Abstract

Tricalcium phosphate (TCP) has many advantages in biomedical applications, especially in teeth and bones, and therefore many researchers focused on enhancing the properties of this material by different methods. Because of the importance of the cerium in repairing the performance of cells in the human body, this work aims to substitute the cerium in TCP structure to give better properties. Coating of Ce/TCP on SS 316L was applied by radio frequency (RF) sputtering technique. This coating was characterized by XRD, FESEM/EDS with EDS mapping, AFM, and electrochemical analysis. These techniques confirm the presence of Ce with TCP in the deposited layer and the SEM gave a more compact layer with higher roughness and lower average diameter. EDS mapping shows the presence of suggested metal ions in the coating. A theoretical study by DFM was done to illustrate the substitution of Ce in the lattice structure and stable sites for accommodation. Electrochemical studies showed that the presence of the coating layer improves corrosion resistance with 91 % protection efficiency.

Keywords

Biomaterials; tricalcium phosphate; Ce substitution; thin-film sputtering; stainless steel

Introduction

The aging of the population is connected with an increase in the number of people with significant joint pathologies. Diseases of the musculoskeletal system are one of the causes of patients' long-term incapacity. Endoprosthesis is one of the most commonly utilized techniques for

repairing fractures of heavy skeletal and bone components such as the spine, knee, and hip joints. The repairing process can be achieved *via* implants, such as 316L stainless steel (SS). 316L SS possesses mechanical properties equivalent to human bones and far lower cost than titanium implants. It also possesses good corrosion resistance in human fluids, as well as formability, durability, and strength. On the other hand, the release of poisonous metallic ions from the 316L SS implant surface into a body has a negative effect on the surrounding tissues. A possible method for reducing implant adverse effects is to create materials that are more compatible with the human body. In other words, bioactive material modification of the implant surface is a good strategy for reducing ion release and improving the corrosion resistance of 316L SS implants [1,2].

Bone tissue is a biomechanical structure composed of specialized cells surrounded by a mineralized matrix that is responsible for producing the essential anchoring for cellular regeneration. This structure is composed mostly of a mineral component (about two-thirds), an organic matrix (about one-third), and a cellular component (less than 2 %). The mineral (inorganic portion) is composed of calcium salts, such as calcium phosphate (around 90 %), calcium carbonate (around 10 %), and calcium fluoride (around 0.3 %). The combination of these compounds provides the bone with resistance to load and compressive forces [3]. Calcium phosphate, which is the main material, refers to an important implant ceramic for bone repair and augmentation due to its excellent biocompatibility and compositional similarity to natural bones. Also, it has the ability for resorption *in vivo* within a few months and works in the growth of bone cells. Tricalcium phosphate (TCP) has been studied actively as a bioresorbable material among bioceramics and is primarily used in orthopedic and maxillofacial implant surgery as a temporary support scaffold. It is important to control the solubility of TCP when used as *in vivo* bone substitution material. Calcium phosphate received attention in many studies to improve material properties as a coating and also to insert other metals into the crystal structure of TCP. Calcium phosphate films were deposited on titanium [4] and Ti-6Al-4V [5] by radiofrequency (RF) magnetron sputtering, and the calcination of calcium phosphate ceramics at 200, 400, 600, 800 and 1000 °C was observed using XRD [6]. Also, calcium phosphate was deposited by RF magnetron sputtering onto 316L SS [7-9]. In addition, the deposition of calcium phosphate (Ca-P) coatings on the material of medical implants was studied and the properties of the coating were found to be uniform, dense, and without any visible defects [10].

A tiny amount of inorganic metal ions such as zinc (Zn), samarium (Sm), strontium (Sr), barium (Ba), and others have been reported to be substituted into the TCP structure to generate implant materials with improved osseous integration, inducing ability and corrosion resistance [11,12]. Structural stability and biocompatibility of TCP are improved by the substitution of the metal ion. Bakheet *et al.* [13] showed that pure TCP material has a lower ability to stimulate the growth of natural bone and teeth than needed. They found that the replacement of calcium with magnesium in the matrix of TCP enhances its electronic and optical properties. Naoyuki *et al.* [14] investigated the effects of the substitution of lithium, sodium, and potassium ions at Ca sites in TCP. They found that the solubility of TCP powder doped with metal ions was lower than pure TCP powder, and the solubility decreased with an increase in the amount of metal ions, which can be attributed to an improvement in the crystal structure. Boanini *et al.* [15] stated that tricalcium phosphate (TCP), or β-tricalcium phosphate (β-TCP), is one of the most common bioceramic materials, especially in the presence of active ions, namely strontium and zinc. In their review paper, Sharifah *et al.* [16] concluded that doping of the most common metals into the calcium phosphate phase optimizes its performance as a bone substitute material.

A limited number of works are available about doping cerium (Ce) in TCP structure. Therefore, the current work aims to substitute Ce within the lattice structure of TCP using RF sputtering method to deposit Ce substituted TCP as a film on SS 316L for biomedical applications.

Experimental

Substrate preparation

Stainless steel (SS) 316L specimen was used as a substrate to apply the coating of Ce substituted TCP. The chemical composition of SS 316L specimen was: 0.022 wt.% C, 0.407 wt.% Si, 1.43 wt.% Mn, 0.031 wt.% P, 0.004 wt.% S, 16.98 wt.% Cr, 2.00 wt.% Mo, 11.73 wt.% Ni, 0.234 wt.% Cu and Fe balance. The specimens were cut as square shapes with dimensions of 2 × 2 cm and then grained with SiC paper (600, 800, 1000, and 1200 grit size) and polished with alumina paste. The substrates were ultrasonically cleaned in a diluted acetone bath for 25 min, followed by rinsing in distilled water to ensure that the substrate surface was free from contaminants and acetone residues.

Coating process

Ce substituted TCP thin film was deposited on SS 316L substrate by RF magnetron sputtering at 150 °C (Model No. CRC 600, Serial No. MST-CRC-102510-ND2-MS). CeO_2/TCP target was prepared using commercially available CeO_2 powder (Merck Darmstadt, 99.99 %) and TCP (HIMEDIA, 99.99 %). A pellet of 50 mm diameter and 5 mm thickness was prepared by compacting the powders in a stainless steel pelletizer under 5 tons as pressure by hydraulic press, and then this pellet was inserted into a furnace for sintering at 1100 °C for 3 h. All experiments were carried out under Ar gas to generate plasma in the sputtering chamber with a pressure of 3×10^{-4} mbar, gas flow rate (5 cm^3/min), deposition time (30 min), RF power (150 W) and temperature of substrate (150 °C). The characterization of thin films was done by XRD with copper K-α radiation (k = 0.15418 nm), FESEM/EDS analysis (FEI QUANTA 250, Czech Republic), and AFM exam (SPM 600, Agilent Technologies).

Microhardness for Hydroxyapatite (HA) and Ce/TCP coated specimens was performed using an indenter (HMV- 2, Shimadzu, Kyoto, Japan). For each specimen, five indentations were performed under a load of 200 mg for 15 s. The Knoop hardness number (KHN, kg mm^{-2}) for each specimen was recorded as the average of the five readings.

Microbiological procedure

Biocompatibility was examined by the microorganisms suspended in BHI broth at the temperature of 37 °C and shaked at 250 r.p.m, containing the minimum inhibitory concentration (MIC), the minimum bactericidal concentration (MBC), and dimethyl sulfoxide (DMSO) of 2 % v/v in peptone water to obtain the density of cell at 10^5 - 10^7 colony-forming unit (CFU). The centrifuging was done at 10000 G for 8 min, followed by washing and re-suspending in 1 mL of sterile PBS. Assaying was done by micro-dilution broth susceptibility. To enhance the solubility, all experiments were carried out in Mueller–Hinton broth (MHB) supplemented with 2 % DMSO. The killing percent was measured by a subculture of 20 mL. Each test was repeated at least three times. An antibacterial test was done by BD Biosciences Calibur. CellQuest Pro Software was used depending on light-scatter and fluorescence signals that result from 15 mW laser illumination at a wavelength of 488 nm. These fluorescence signals were collected by FL-1 (BOX) and FL-3 (PI, EB and CTC) bandpass filters. All acquired data were read, analyzed and performed *via* Cell Counter.

Electrochemical and corrosion procedure

Potentiodynamic polarization studies were carried out using a potentiostat apparatus. The procedure was according to ASTM G1-03 & ASTM G3-14. The bare and Ce/TCP coated specimens were used as the working electrodes. The exposed surface area was 0.7 cm^2. The corrosive solution was a simulated body fluid (SBF). The electrochemical 1 L standard cell was used and equipped with the required electrodes. Ag/AgCl (KCl-sat.) was used as a reference electrode. A Haber - Luggin capillary put close to the working electrode was used to reduce solution resistance. The auxiliary electrode was rectangular graphite. The SBF was prepared using Ringer tablet dissolved in 0.5 L of distilled water. The solution was heated up to 120 °C for 15 min, then left for cooling, followed by adding Na_2HCO_3 to obtain a pH of 7.4. Ringer tablets were obtained from Merck Company, Germany.

Tafel polarization was done in two steps; the first is represented by following open circuit potential (E_{OCP}) values after immersion of specimens for one hour in SBF. E_{OCP} values were recorded with respect to Ag/AgCl electrode until steady-state potential. The second step is represented by changing the potential ± 200 mV around the open-circuit potential (OCP) value at the scan rate of 0.5 mV s^{-1} to get corrosion data such as corrosion potential (E_{corr}), corrosion current density (j_{corr}), and Tafel slopes (b_c and b_a). All experiments were achieved at 37 °C in duplicate and the average value was taken for further analysis.

Results and discussion

Characterization and structural considerations

Figure 1 shows the XRD analysis of SS 316 L substrate, which indicates diffraction peaks related to the crystalline phase of stainless steel 316 L according to JCPDS card No. 33-0397 [17]. The substitution was done by adding 90 wt.% cerium oxide to TCP. Figure 1 also illustrates the XRD pattern for Ce/TCP, where the analysis indicates the peaks of the substrate, peak of cerium oxide at 2θ=28.37°, and other peaks that are attributed to the presence of α-Ce according to JCPDS card No. 38-0765 at 2θ values of 32.869 and 47.18°. In this XRD pattern, the separation among phases of started materials is not observed. When substitution of Ce was done, a distorting of the lattice structure can occur, suggesting certain incorporation of the cerium oxide within TCP lattice.

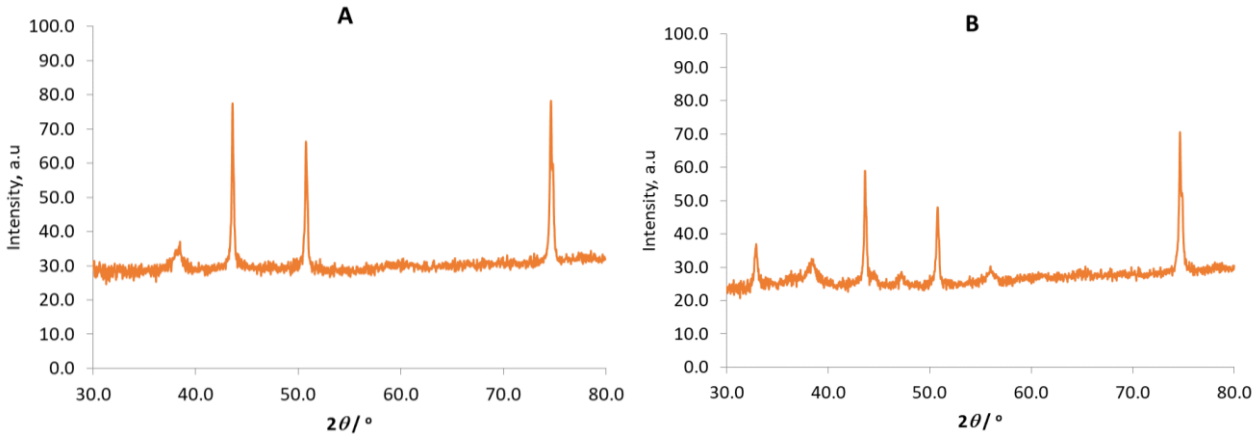

Figure 1. *XRD pattern of (A) SS 316 L and (B) Ce/TCP deposited on SS*

Figure 2A indicates the FESEM/EDS of the polished SS 316L surface with little atmospheric corrosion. Also, this image shows a characteristic inclusion observed on the surface. EDS analysis shows the main elements in SS 316L (Fe, Cr and Ni) in addition to oxygen obtained from the iron oxide layer due to the influence of atmospheric corrosion.

The addition of CeO_2 (90 wt.%) led to a more homogeneous surface (Figure 2B), which is due to the appearance of cerium with calcium phosphate layers, as indicated in XRD analysis at 2θ value ≈28^{o,} in addition to the presence of CaO. The addition of ceria gave a compact layer with more deposited particles due to coverage of the surface by cerium, indicated in EDS analysis by Ce equal to 68.1 wt.% alongside Ca (11.7 wt.%), P (7 wt.%) and O (10.3 wt.%).

EDS mapping of SS 316L and C/TCP coated SS 316L is shown in Figure 3A and B, respectively, revealing the elemental distribution of metal ions in the substrate (Cr, Fe, Ni and O) and Ce/TCP coating as calcium (Ca) and oxygen (O), in addition to cerium (Ce) and phosphor (P) confirming the substitution of cerium in TCP.

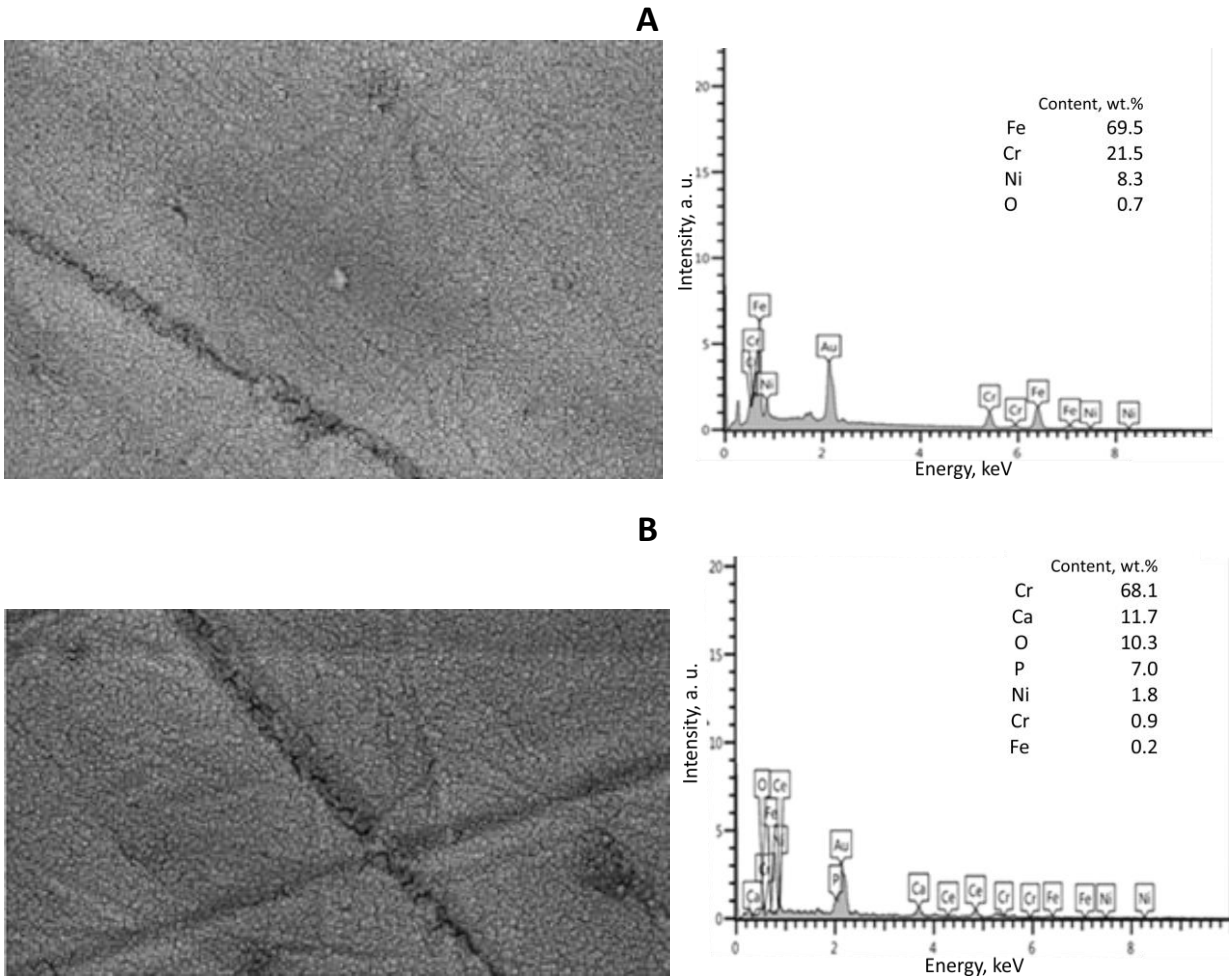

Figure 2. *FESEM/EDS of (A) SS 316L substrate and (B) Ce/TCP deposited on SS 316L*

AFM images indicate the topography of the coated surface. 2D and 3D images for SS 316L surface are shown in Figure 4A, indicating a smooth surface with very little roughness value (around 1.4 nm) due to little atmospheric corrosion and low summit (7.42 nm). Ce/TCP coating gave higher roughness equal to (4.49 nm) due to disorder of lattice structure because of insertion of Ce^{3+} and Ce^{4+} ions within some sites of TCP structure. As shown in Figure 4B, the maximum height was reached at 18.34 nm.

The average diameter was reduced from 83.85 to 37.73 nm for the distribution of particles on the surface, what means that the substitution fills all holes in the crystal structure of TCP as shown in Figure 5.

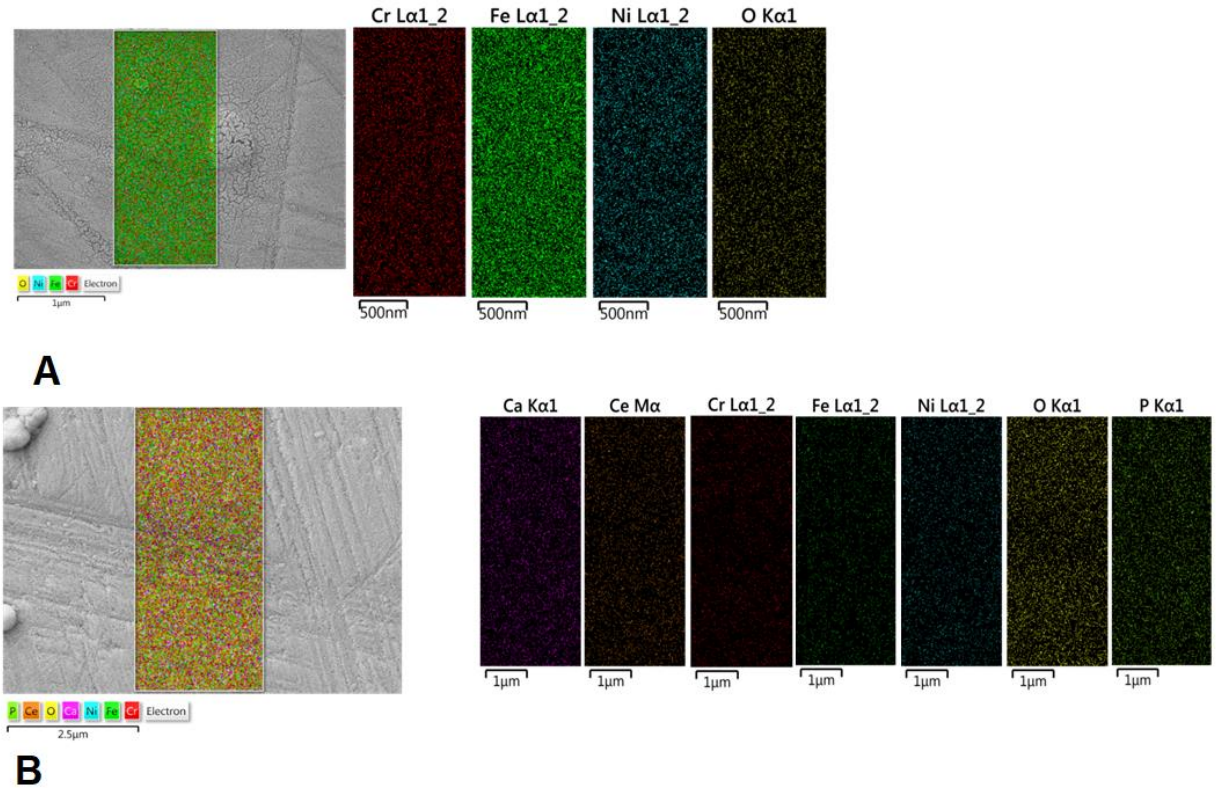

Figure 3. *EDS mapping of (A) SS 316L and (B) Ce/TCP deposited on SS 316 L*

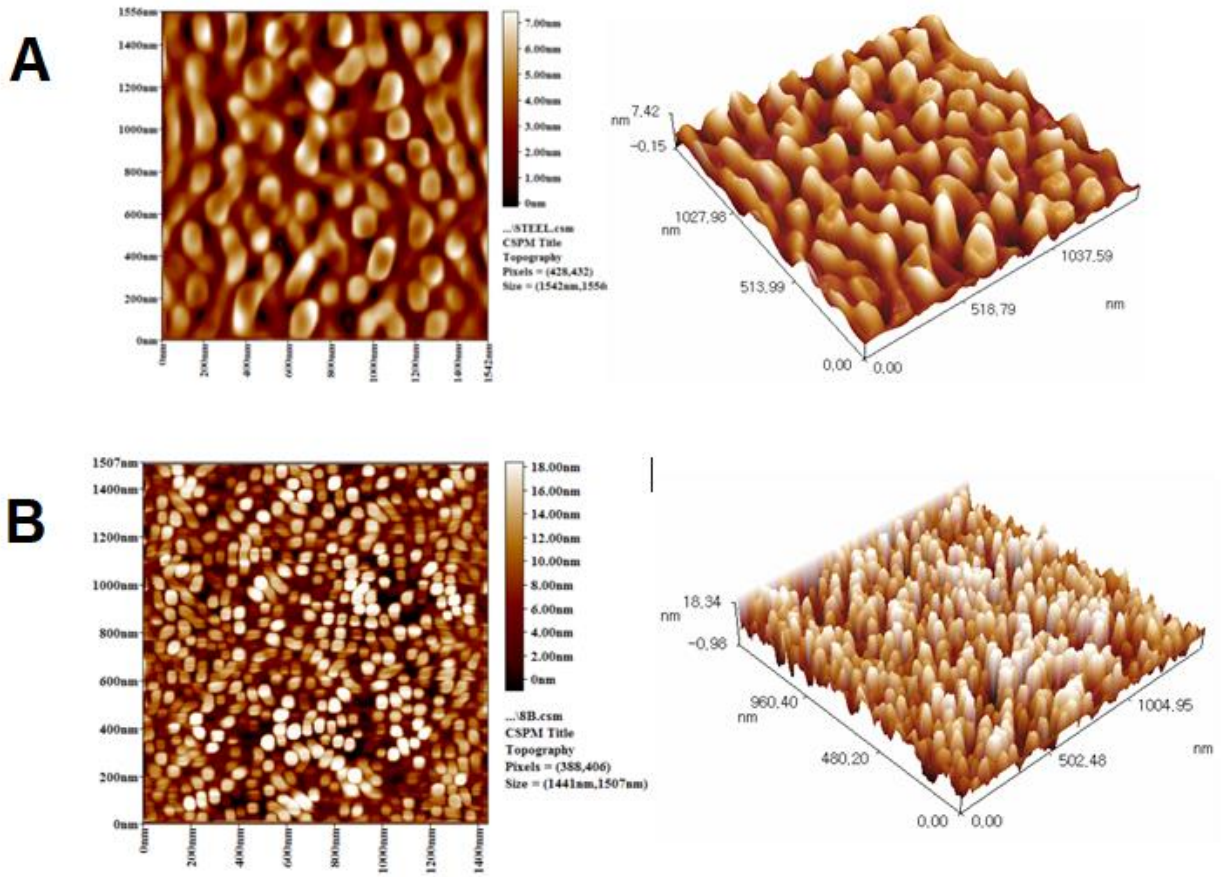

Figure 4. *AFM images of (A) SS 316 L and (B) Ce/TCP deposited on SS 316 L*

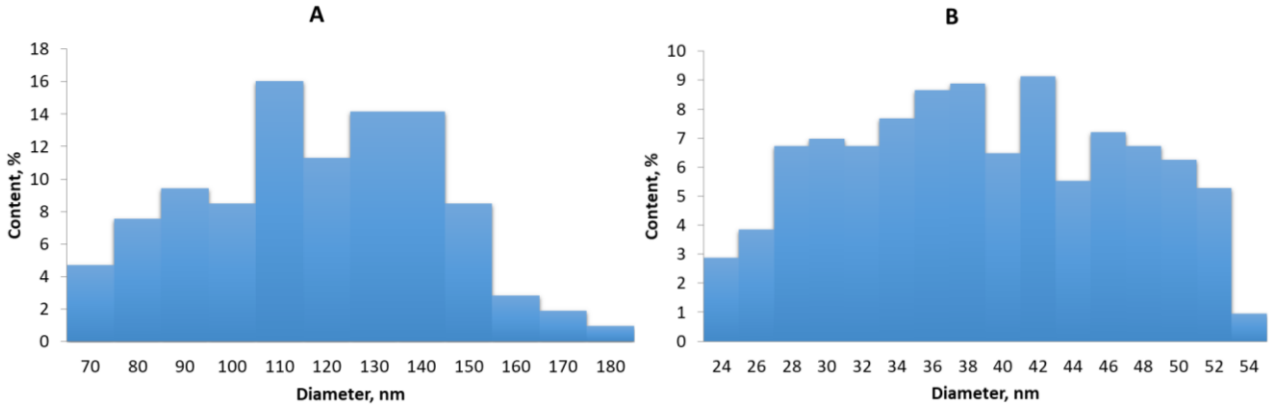

Figure 5. *Distribution of particle sizes for (A) SS 316 L and (B) Ce/TCP deposited on SS 316 L*

Mechanism of substitution

It has already been suggested that TCP has five distinct Ca sites with octahedral coordination suitable for cationic substitution, where monovalent ion substitution prefers substitution at the Ca(4) site, bivalent ion substitution prefers Ca(4) and Ca(5) sites, while trivalent ion substitution could not simply substitute at Ca(4) or Ca(5) sites [18]. On the other hand, the largest lanthanide ions, such as La, Ce, Pr, and Nd prefer Ca(3) site [19]. In another study, the authors indicated that the substitution of smaller size divalent ions can accommodate at the Ca(5) site, whereas larger size ions prefer the Ca(4) site [20,21] due to differences in bond length of these five different sites of calcium. In another work, the X-ray diffraction data illustrated six sites of Ca atoms in TCP structure that can be accommodated as 1, 3, and 5, and 2, 4, and 6, respectively, according to equivalent configurations. Theoretically, the uniform distribution of calcium vacancies has to be stable and every Ca atom in the structure has at least one neighboring vacancy associated with defects like electronic states [22].

For trivalent ions such as cerium, the substitution mechanism may be complex due to the size and valence effect as $2M^{3+}=2Ca^{2+}+v$, where M^{3+} stands for Ce^{3+} and v denotes a vacancy [23]. Depending on the mean bond length of Ca–O, Ce^{3+} prefers Ca(3). From DFM calculations, the substitution can be done according to energy levels as accommodation. The theoretical calculations for optimized structures were performed for the vacuum medium [24,25]. The structure of TCP (Figure 6A) was calculated by using (UFF/ZDO) method with Gaussian 09 software [26,27]. The PM6 semi-empirical method was used to determine the total electron density (TED) [28,29]. The red color region indicates a high electronic density area, followed by the orange color region, which represents lower electronic density than in the red region, while the blue color area represents a low electronic density area. Oxygen and phosphor with high electron density (Figure 6B) present the electron density above the crystal TCP.

The theoretical discussion for CeO_2/TCP coating suggests the perfect position of Ce in the lattice structure of TCP as follows: total energy (E_t) of TCP without Ce is (5.6807 a.u.) and with Ce (6.9299, 13.7252 a.u.) as shown in (Figure 6C and D) for two positions. According to E_t values, Ce in the structure (***a*** position) is more acceptable than (***b*** position), *i.e.,* Ce prefers the sites 1, 3 and 6 rather than 2, 4 and 5. The distance between Ce and Ca was very close in TCP, indicating stability. The bond length of (Ce–Ca) is in the range of (0.22 to 0.319 nm) and (Ce–O) is about 0.19 to 0.29 nm. In 2016, a theoretical study of Mg substituted β-TCP to investigate the improvement of β-TCP biomaterial in bones and teeth replacements was made by (DFT) [17]. Recently, in 2019, It was found that replaced calcium atoms with rare earth elements (REEs, La, Ce, Nd and Y) in the lattice structure of fluorapatite ($Ca_{10}F_2(PO_4)_6$), taking into account the Fermi level of these elements that have 5d, 4f, 4f and 4d level, respectively.

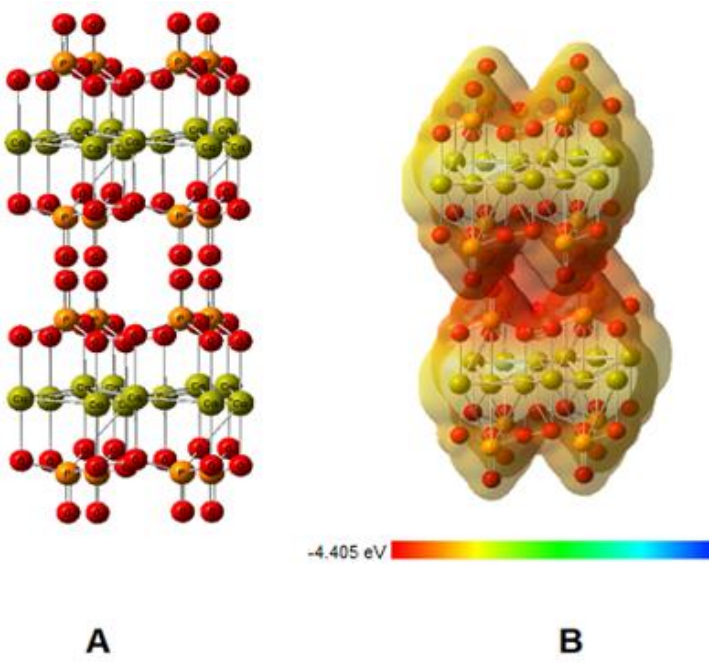

Figure 6. *(A) TCP structure without Ce element; (B) TED map for TCP structure*

Biological considerations

Figure 7 shows the biocompatibility test for Ce substitution TCP coating compared with the most known ceramic material in bio-applications (hydroxyapatite). This figure indicates that the biocompatibility of Ce/TCP coating is greater than hydroxyapatite (HA) coating. Also, the results showed that after 24 h of incubation, the material surface was completely covered by the cell layer, and the coverage increased with increasing the incubation time.

The antibacterial tests were also carried out. The results showed that the antibacterial response for Ce/TCP coating is more than for uncoated SS 316L. More than 20 % of bacteria died in the case of Ce/TCP coating as compared with SS 316L. A reason may be the incorporation of mineral cerium, which plays a vital role in enhancing antibacterial activity.

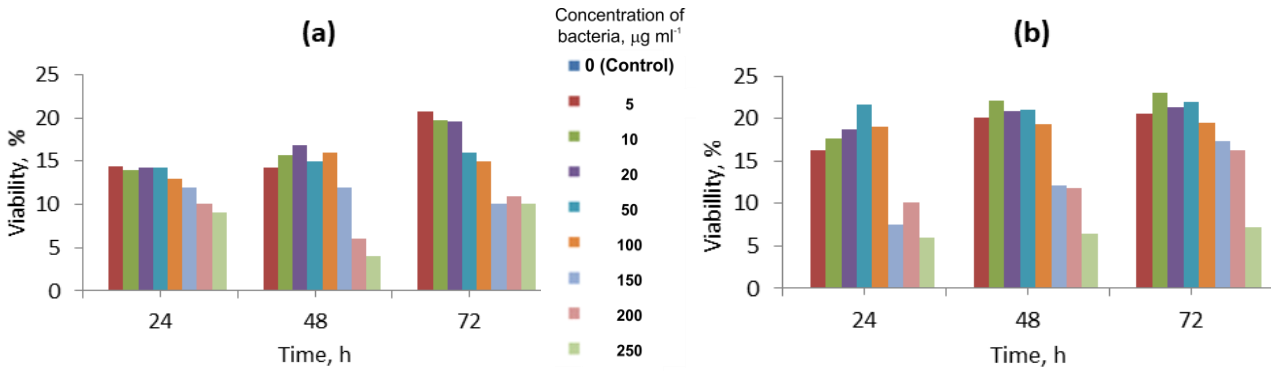

Figure 7. *Biocompatibility of (a) HA and (b) Ce/TCP deposited on SS 316 L at different concentrations of bacteria*

Microhardness considerations

Microhardness examination for Ce/TCP coated SS 316L was compared with HA-coated specimen, and the results are shown in Table 1. The substitution of Ce in TCP structure led to increasing microhardness due to filling the vacancies in the structure by other elements to get compact arrays of atoms.

Table 1. *Microhardness data for HA and Ce/TCP coatings on SS 316L in different media at initial conditions of time and after 5 days.*

Specimen	Hardness, HV					
	Water		PBS		Acetone	
	Initial	5 days	Initial	5 days	Initial	5 days
HA coated SS 316L	88.1	59.3	89.2	77.0	83.4	68.2
Ce/TCP coated SS 316L	114.4	102.6	112.0	98.4	119.6	91.8

Electrochemical considerations

The open-circuit potential (OCP) and polarization curves for uncoated and (Ce/TCP) coated SS 316L specimens in the simulated body fluid (SBF) at 37 °C are shown in Figures 8 A and B, respectively.

Corrosion behavior is an important factor in predicting the validity of any bioimplant because it represents the success of the implantation. In Figure 8A, the potential-time measurements of uncoated and Ce/TCP coated SS 316L were slightly shifted toward negative values with increasing time. Also, E_{OCP} value for Ce/TCP coated sample was more positive (nobler) than for the uncoated one.

The relationship between potential and current density represents the electrochemical behavior of metal in a given environment and is called the polarization curve or Tafel plot. Figure 8B shows the polarization curves of uncoated and Ce/TCP coated specimens in SBF at 37 °C. Again, the corrosion potential (E_{corr}), and corrosion current density (j_{corr}), were affected in the presence of the coating layer. The electrochemical parameters, E_{corr}, j_{corr}, and Tafel slopes (b_a and b_c), are listed in Table 2.

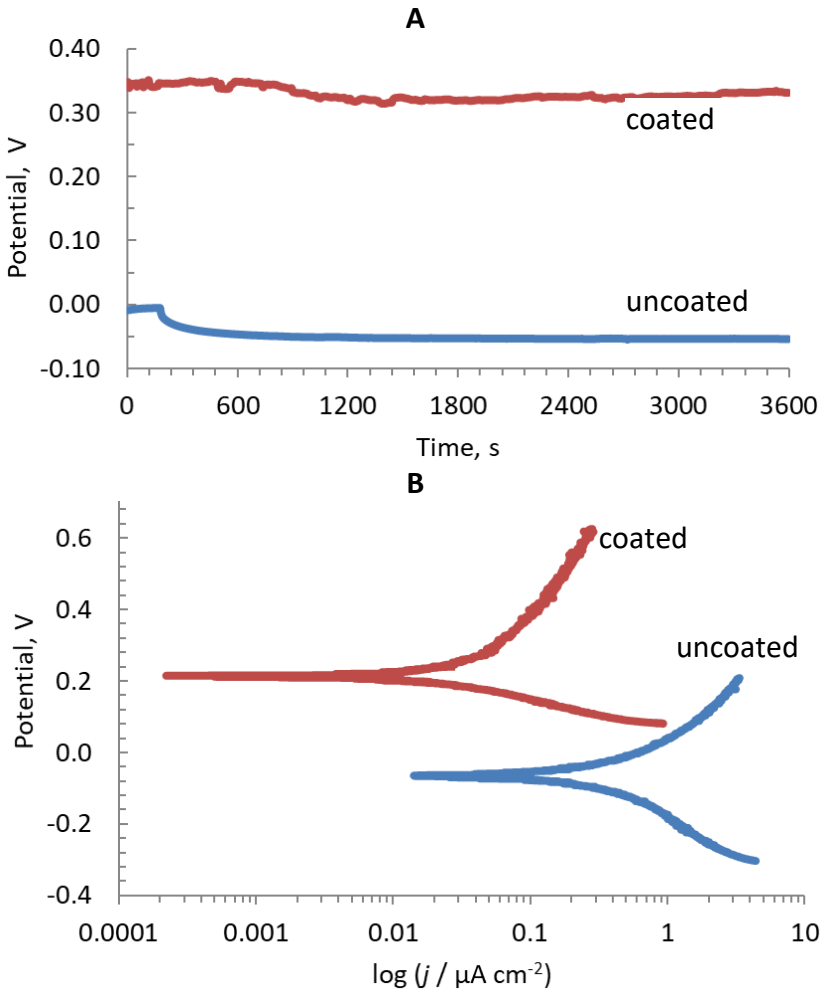

Figure *8. Open circuit potential and (B) polarization curves for uncoated and Ce/TCP coated SS 316L specimens in simulated body fluid (SBF) at 37 °C.*

Table 2. *Electrochemical parameters of uncoated and Ce/TCP coated SS 316L*

Parameter	Stainless Steel 316L	Ce/TCP coated SS 316L
E_{OCP} / mV	-56.6	+330.8
E_{corr} / mV	-56.00	+226.219
j_{corr} / μA cm^{-2}	0.1875	0.01687
$-b_c$ / mV dec^{-1}	138.912	99.799
b_a /mV dec^{-1}	102.276	104.005
C_R / mm year^{-1}	8.75	0.79
R_p / kΩ cm^2	0.136	1.310
PE, %	-	91
PP, %	-	0.018

The variation in the E_{corr} value shows the variation in cathodic and anodic sites on the surface and may be different due to the porosity of the coating layer. The important indication about corrosion is related to the j_{corr} value. The decreasing of j_{corr} value for Ce/TCP coated specimen compared with uncoated SS 316L is occurring through the role of cerium ions with two oxidation states (*i.e.,* Ce^{3+} and Ce^{4+}) within the coating, which have the ability to supply oxygen to vacancies and cover the metallic surface by passive film, decreasing thus the metal corrosion rate (C_R). Cathodic and anodic Tafel slopes (b_c and b_a) determine the mechanism and kinetics of the corrosion reaction, and there are variations in these slopes. A higher cathodic Tafel slope (b_c) was indicated for Ce/TCP coated SS 316L, which means that the cathodic reaction at cathodic sites is faster in producing hydroxyl ions, supporting the formation of passive film on the surface. On the other hand, the lowest anodic Tafel slope (b_a) was for Ce/TCP coated SS 316 L, and this means that the turn to the passive region is fast due to increasing the ceria on the surface and the increasing substitution of ceria in TCP structure enhancing the passive film on the surface.

Tafel slopes and corrosion current density are used to calculate the polarization resistance (R_p) according to the following formula:

$$R_p = \frac{b_c b_a}{2.303 i_{corr}(b_c + b_a)} \quad (1)$$

The polarization resistance values in Table 2 indicate a higher R_p value for Ce/TCP coated SS 316 L. Corrosion current density for uncoated and coated specimens was also used to calculate the protection efficiency (*PE*) as follows:

$$PE = \left(1 - \frac{j_{corr,coated}}{j_{corr,uncoated}}\right)100 \quad (2)$$

The value of protection efficiency was calculated as 91 % for Ce/TCP coated SS 316 L. All ceramic coatings have porosity, but lower porosity means a more compact layer. The porosity % (*PP*) for a coating can be calculated from the following formula:

$$PP = \frac{R_{p,uncoated}}{R_{p,coated}} 10^{\frac{-\Delta E}{b_a}} 100 \quad (3)$$

where $R_{p,uncoated}$ and $R_{p,coated}$ are polarization resistances of the uncoated and the coated specimens, respectively, ΔE is the corrosion potential difference between the coated and uncoated specimen, while b_a is anodic Tafel slope for the uncoated specimen. Porosity data shows a low porosity value for Ce/TCP coating due to deposition of α-cerium.

Conclusions

The following points were concluded from the present work:

1. Ce/TCP coating has been applied successfully on 316L SS surface using radio frequency sputtering technique.
2. XRD, FESEM/EDS with EDS mapping, and AFM analysis confirmed the presence of Ce and TCP in the deposited layer.
3. SEM images of Ce/TCP coating showed a more compact layer with higher surface roughness and lower average particles diameter.
4. EDS mapping showed the presence of Ce ions in the coating.
5. A theoretical study by density function theory illustrated the substitution of Ce into the lattice structure and stable sites for accommodation.
6. Electrochemical studies showed that the presence of Ce/TCP coating layer improves corrosion resistance in simulated body fluid (SBF) with 91 % protection efficiency.

References

[1] H. Qiao, H. Xiao, Y. Huang, C. Yuan, X. Zhang, X. Bu, Z. Wang, S. Han, L. Zhang, S. Su, X. Zhang, *Surface and Coatings Technology* **364** (2019) 170-179. https://doi.org/10.1016/j.surfcoat.2019.02.089

[2] D. Zhang, H. Zhang, J. Wen, J. Cao, *IOP Conference Series*: *Earth and Environmental Science* **233(2)** (2019) 022007. https://doi.org/10.1088/1755-1315/233/2/022007

[3] W. Aperador, E. Ruíz, G. Orozco Hernández, J.C. Caicedo, C. Ameya. *MOJ Applied Bionics and Biomechanics* **2(2)** (2018) 157-162. https://doi.org/10.15406/mojabb.2018.02.00059

[4] T. Narushima, K. Ueda, T. Goto, H. Masumoto, T. Katsube, H. Kawamura, Ch. Ouchi, Y. Iguchi, *Materials Transactions* **46(10)** (2005) 2246-2252. https://doi.org/10.2320/matertrans.46.2246

[5] A.R. Boyd, B.J. Meenan, N.S. Leyland, *Surface and Coatings Technology* **200(20-21)** (2006) 6002-6013. http://dx.doi.org/10.1016%2Fj.surfcoat.2005.09.032

[6] D. K. Pattanayak, R. Dash, R. C. Prasad, B. T. Rao, T. R. Rama Mohan, *Materials Science and Engineering: C* **27(4)** (2007) 684-690. https://doi.org/10.1016/j.msec.2006.06.021

[7] J. A. Toque, M. Hamdi, A. Ide-Ektessabi I. Sopyan, *International Journal of Modern Physics* **23(31)** (2009) 5811-5818. https://doi.org/10.1142/S021797920905479X

[8] J.A. Toque, M.K. Herliansyah, M. Hamdi, A. Ide-Ektessabi, I. Sopyan, *Journal of the Mechanical Behavior of Biomedical Materials* **3(4)** (2010) 324-330. http://eprints.um.edu.my/id/eprint/14727

[9] K.-Y. Hung, H.-C. Lai, H.-P. Feng, *Coatings* **7(8)** (2017) 126. https://doi.org/10.3390/coatings7080126

[10] M. Montazerian, F. Hosseinzadeh, C. Migneco, M. Fook, F. Baino, *Ceramics International* **48(7)** (2022) 8987-9005. https://doi.org/10.1016/j.ceramint.2022.02.055

[11] D. S. Morais, S. Fernandes, P. S. Gomes, M. H. Fernandes, P. Sampaio, M. P. Ferraz, J. D. Santos, M. A. Lopes, N. S. Hussain, *Biomedical Materials* **10(5)** (2015) 055008. https://doi.org/10.1088/1748-6041/10/5/055008

[12] D. Sivaraj, K. Vijayalakshmi, *Ultrasonics Sonochemistry* **59** (2019) 104730. https://doi.org/10.1016/j.ultsonch.2019.104730

[13] A. M. A. Bakheet, M. A. Saeed, R. Sahnoun, A. R. M. Isa, L. Mohammed, T. Mahmood, *Jurnal Teknologi* **78(3)** (2016) 167-172. http://dx.doi.org/10.11113/jt.v78.7487

[14] N. Matsumoto, K. Yoshida, K. Hashimoto, Y. Toda, *Journal of the Ceramic Society of Japan* **118(1378)** (2010) 451-457. https://doi.org/10.2109/jcersj2.118.451

[15] E. Boanini, M. Gazzano, C. Nervi, M. R. Chierotti, K. Rubini, R. Gobetto, A. Bigi, *Journal of Functional Biomaterials* **10(2)** (2019) 20. https://doi.org/10.3390/jfb10020020
[16] S. Adzila, M. Murad, I. Sopyan, *Recent Patents on Materials Science* **5(1)** (2012) 18-47. http://dx.doi.org/10.2174/1874464811205010018
[17] G. Silva, M. R. Baldissera, E. de Sousa Trichês, R. Cardoso, *Materials Research* **16(2)** (2013) 304-309. https://doi.org/10.1590/S1516-14392012005000182
[18] S. Basu, B. Basu, *Journal of Asian Ceramic Societies* **7(3)** (2019) 265-283. https://doi.org/10.1080/21870764.2019.1636928
[19] A. Bessière, R. A. Benhamou, G. Wallez, A. Lecointre, B. Viana, *Acta Materialia* **60(19)** (2012) 6641-6649. https://doi.org/10.1016/j.actamat.2012.08.034
[20] S. Kannan, F. Goetz-Neunhoeffer, J. Neubauer, S. Pina, P. M .C. Torres, J. M. F. Ferreira, *Acta Biomaterialia* **6(2)** (2010) 571-576. https://doi.org/10.1016/j.actbio.2009.08.009
[21] S. Kannan, F. Goetz-Neunhoeffer, J. Neubauer, J. M. F. Ferreira, *Journal of the American Ceramic Society* **94(1)** (2011) 230-235. https://doi.org/10.1111/j.1551-2916.2010.04070.x
[22] X. Yin, M. J. Stott, A. Rubio, *Physical Review B* **68(20)** (2003) 205205. https://doi.org/10.1103/PhysRevB.68.205205
[23] K. Yoshida, H. Hyuga, N. Kondo, H. Kita, M. Sasaki, M. Mitamura, K. Hashimoto, Y. Toda, *Journal of the American Ceramic Society* **89(2)** (2006) 688-690. https://doi.org/10.1111/j.1551-2916.2005.00727.x
[24] F. Kazemi, A. R. Kiasat, S. Ebrahimi, *Synthetic Communications* **33(6)** (2006) 999-1004. https://doi.org/10.1081/SCC-120016364
[25] P. Hohenberg, W. Kohn, *Physical Review* **136(3B)** (1964) B864-B871.
[26] I. Komaromi, J.M.J. Tronchet, *Journal of Molecular Structure (Theochem)* **395-396** (1997) 15-27.
[27] R. E. Plata, D. A. Singleton, *Journal of the American Chemical Society* **137(11)** (2015) 3811-3826. https://doi.org/10.1021/ja5111392.
[28] E. A. Yaqo, R. A. Anee, M. H. Abdulmajeed, I. H. R. Tomi, M. M. Kadhim, *ChemistrySelect* **4(34)** (2019) 9883-9892. http://dx.doi.org/10.1002/slct.201902398
[29] X. Wang, Q.-Zhang, S.-Mao, W. Cheng, *Minerals* **9(8)** (2019) 500. https://doi.org/10.3390/min9080500